Characterizing 60 GHz Patch Antenna Segments for Fully Digital Transceiver

Jaakko Haarla*, Vasilii Semkin†, Kai Zheng‡, Aditya Dhananjay‡, Marco Mezzavilla‡, Juha Ala-Laurinaho*, and Ville Viikari*

*Department of Electronics and Nanoengineering, Aalto University, Espoo, Finland. {firstname.lastname}@aalto.fi
†VTT Technical Research Centre of Finland, Finland, {vasilii.semkin}@vtt.fi
‡Tandon School of Engineering, New York University. {kz938, avd263, mezzavilla}@nyu.edu

***Abstract*—In this work, we present the simulation and measurement results of patch antenna elements operating at 60 GHz for future integration with fully digital transceiver. The antennas are fabricated on Rogers 4350B substrate of 168 µm thickness and their radiation patterns are measured both in the anechoic chamber and planar near-field range. In addition, different types of transmission lines are designed and fabricated. Results for both patch antennas and transmission lines show rather good agreement between simulation and measurements. The measured -10 dB bandwidth of single element is 1.76 GHz around center frequency of 60.3 GHz. In the future, 1x4 patch antenna array will be integrated with the four channel software-defined radio.**

***Index Terms*—antenna array, millimeter wave, software-defined radio, 60 GHz, fully digital.**

I. Introduction

The existing wireless bands (lower than 6 GHz) have limited amounts of spectrum, and are severely congested due to the sheer number of different networks that operate there (WiFi, 3G, 4G, and public-safety networks). In order to achieve rates of multiple Gbp/s it is necessary to consider higher frequency ranges, where there is an abundance of available spectrum [1]. The millimeter-wave (mmWave) bands (∼30-300 GHz) are particularly well suited to alleviate this *spectrum crunch*, and meet the data requirements that are demanded [2]. Particularly, the unlicensed frequency range from 57-64 GHz is of interest and is considered for wireless multi-gigabit communications [3].

While these mmWave bands have abundant spectrum, the radio waves are not as *well-behaved* as those in the traditional sub-6 GHz bands. The isotropic path losses are significantly higher, thereby rendering omni-directional transmissions and receptions infeasible. To overcome these path losses, the signals need to be focused in narrow beams using active or passive beamforming techniques; these beams might need to be switched at microsecond-level time-scales, thereby necessitating the use of electronically steerable antenna arrays [4].

Rapidly developing electronics and technologies allow realization of the SDR platforms for mmWave frequencies [5]. Software-defined radios (SDRs) are the fundamental tool used by wireless systems engineers to build prototypes or research demonstrations. In [6], authors have presented fully digital beamforming receiver for 5G mobile communication at 28 GHz. In contrast, we are targeting to build fully digital SDR transceiver operating at 60 GHz [7]. The envisioned SDR system consists of two main parts: an off-the-shelf Xilinx KC705 FPGA board, and transceiver board that is mated with the FPGA board. The combination of FPGA and transceiver board with a host computer represents a powerful SDR system. Critically, the SDR system implements a *fully-digital* mmWave transceiver with four channels, operating in the unlicensed V-band (57-64 GHz). The block diagram of the planned SDR is presented in Fig. 1. Specifically in this work, we are focusing only on the mmWave antenna design and characterization.

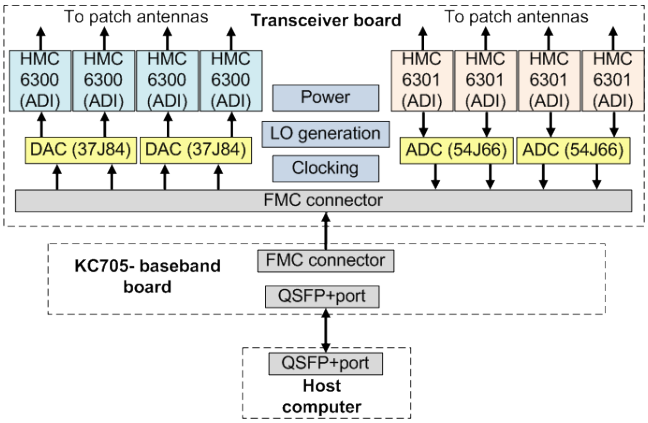

Fig. 1. Schematic diagram of the planned SDR Prototype with 4 channels, operating at 60 GHz, fully-digital.

The board design was performed at New York University[1], while the antenna, transmission line, and balun design was performed by the co-authors currently at Aalto University and VTT Technical Research Centre. All hardware design schematics have been published on GitHub under the MIT license[2]. The technical focus of this paper is on the challenges involved with high-frequency (mmWave) board design, along with RF-feed network and antenna array integration.

[1]Disclosure: The NYU co-authors are involved with a startup Pi-Radio, which is working on SDR systems (with a different architecture based on the Xilinx RFSoC.)

[2]http://bit.ly/FullyDigitalSDR60GHz

Authorized licensed use limited to: Univ of Calif San Diego. Downloaded on January 03,2025 at 18:45:55 UTC from IEEE Xplore. Restrictions apply.

TABLE I
MATERIALS PARAMETERS USED IN SIMULATIONS

	Diel. const. ϵ_r	loss tan. $\tan\delta$	conductivity $\frac{S}{m}$	surface roughness µm
4350B	3.66	0.0037	-	-
copper top	-	-	5.8e7	0.4
copper diel.	-	-	5.8e7	3.2
soldermask	3.5	0.025	-	-
gold	-	-	4.56e7	0
brass	-	-	2.74e7	0
teflon	2.1	0.0002	-	-

II. PROTOTYPE DESIGN

Goal of the paper is to present simple building blocks that can be used for a 60-GHz antenna array in the envisioned SDR platform. The conductor-backed coplanar waveguide (CBCPW) transmission line is used to minimize the interference from other components by having continuous ground around the whole RF section. The ground-plane of the CBCPW on the top layer is connected to the ground plane of the PCB through via-stitching [8]. However, via stitching has a drawback: they create a ground barrier that split the board into smaller sections, which prevent efficient RF routing. This problem can be solved by using micro-, blind-, and buried vias. This, however, increases the manufacturing costs of the PCB. In this paper, we study how removing a small part of these vias affect the signal paths across the RF traces. This enables easier routing of two RF networks on different sides of the printed circuit board (PCB), e.g., LO and RF distribution.

At 60 GHz the minimum via clearance of 450 μm is significant when compared to the wavelength ($\lambda = 2.62$ mm with PCB dielectric constant of 3.66). Under $\frac{\lambda}{4}$ is preferred with longer transmission lines [9]). In this paper, we are interested in removing small sections while keeping the rest of the structure with dense via stiching.

The CBCPW dimensions were set to match a 50-Ω transmission line with minimal gap and via spacing: Line width = 292μm, gap width = 150μm, via from gap = 150 μm and via spacing = 750 μm. Fig. 2a and Fig. 2b shows the designed CBCPW. Missing via sections were designed (seen in Fig. 3) with one or two, one and both-sided vias missing.

Curved CBCPW (Fig. 2c) uses same previously specified dimensions with a 2.0-mm radius of curvature. Via spacing in the curve section was set by splitting the 90° arc into equal parts that minimize the via spacing limited by the manufacturing process.

Rat-race balun was designed in case 100-Ω balanced feed line is needed for the RF-IC [10]. Balanced side of the structure is set to match 0.5 mm pitch. Balun has a 340-µm wide 50-Ω microstrip line and 1.0-mm long CBCPW-to-microstrip line tapering to interface with other CBCPW parts. In order to measure the rat race balun using two channel test setup, a back-to-back structure was manufactured.

A 60 GHz patch antenna array was designed by placing four similar patch antennas $\frac{\lambda}{2}$ apart to avoid grating lobes [11]. A ground ring with a via fence is implemented around

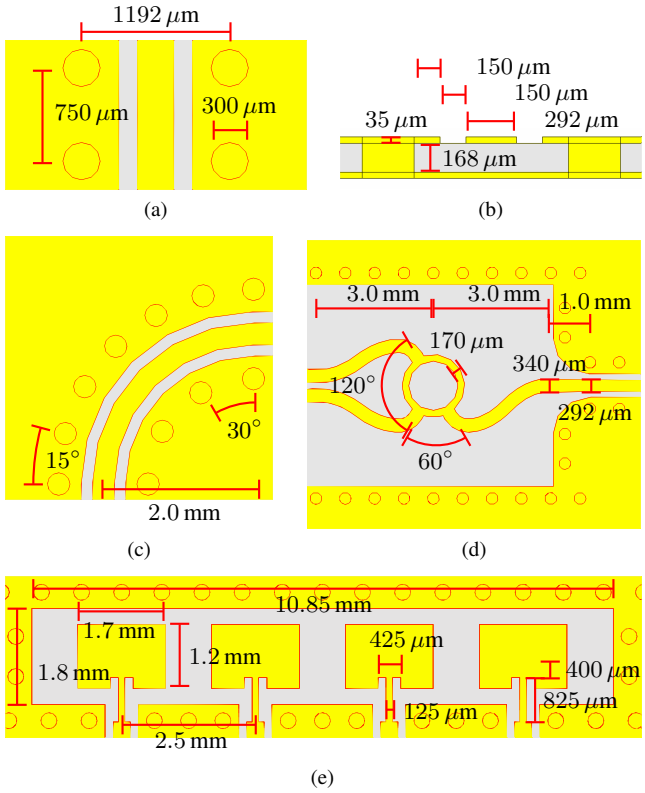

Fig. 2. Designed structures: (a) CBCPW top view, (b) CBCPW side view, (c) curved CBCPW, (d) the rat race balun, and (e) antenna array.

the patch array. The distance between these was minimized without influencing the resonance frequency of the patch array. Antenna feed is a combination of $\frac{\lambda}{4}$ impedance transformer and an edge feed inset to match the 50-Ω CBCPW to the patch. A four-port feed network with 1.8-mm spacing for the connectors was implemented from previously introduced parts.

The prototype layer stack-up is 4-layer PCB: 168 μm Rogers 4350B as the RF substrate on the top and two 0.6-mm FR4 layers as the for structural support. In the simulations, only 4350B with its copper layers was included. The surface roughness was included in the simulations [12]. The material parameters used in the simulations are listed in Table I.

III. SIMULATION AND MEASUREMENT RESULTS

The fabricated prototype is split into numbered sections according to Fig. 3 and are referred by these numbers in following sections. The board includes: two corner transitions (1, 2), back-to-back rat-race balun (3), 1x4 antenna array (4), and straight CBCPW sections: a reference and four with missing via(s) (5-9). The simulation of each structure consists of only its functional parts, near environment and the connector models.

Prototype was measured using Anritsu MS4647B VNA and Southwest Microwave 1892-04A-6 1.85-mm end-launch connectors. Two-port S-parameters were measured for structures 1-3 and 5-9. Due to limited number of connectors, only two antennas were measured at a time, however, all combinations

Authorized licensed use limited to: Univ of Calif San Diego. Downloaded on January 03,2025 at 18:45:55 UTC from IEEE Xplore. Restrictions apply.

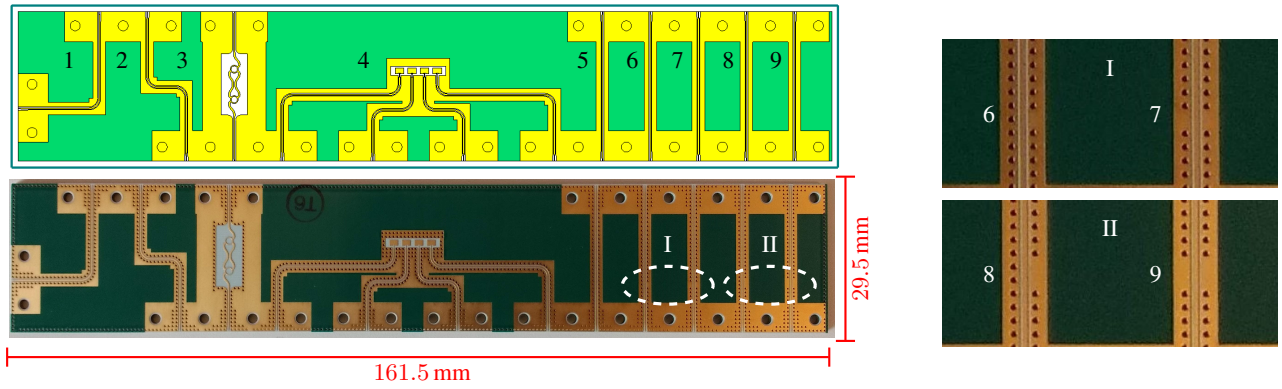

Fig. 3. CST model and manufactured prototype are shown. Individual designs are numbered and missing via sections are shown in detail in I and II.

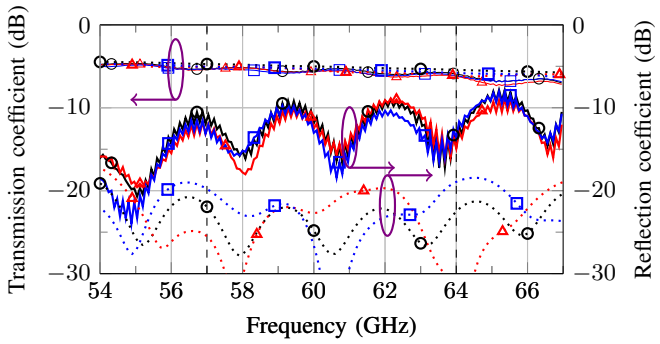

Fig. 4. Simulated (· · ·) and measured (−) S-parameters for straight sections. (5)-reference section ◯, (7)-one via pair missing 7 △, and (9)-two via pairs missing □.

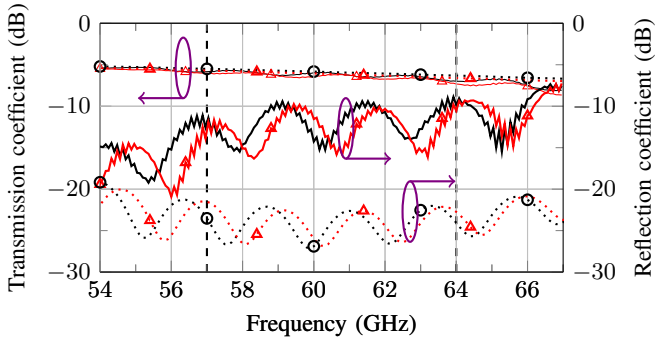

Fig. 5. Simulated (· · ·) and measured (−) S-parameters for (1)-single curve section ◯ and (2)-dual curve section △.

were measured. Measured ports have connectors and two other ports are open.

The prototype had a 200-µm gap between the edge of the board and the copper layers due to manufacturing. In simulations, these layers were assumed to reach the edge and touch the connector. Approximately 100 µm of the board edge was removed by sanding to minimize the gap. The remaining gap effects the matching between the connector and the PCB and thus causes changes in insertion loss and reflection coefficients in the following measurements.

TABLE II
TRANSMISSION COEFFICIENTS AT 57-64 GHZ AND LENGTHS OF THE MEASURED STRUCTURES

	min$\lvert S_{21}\rvert$	max$\lvert S_{21}\rvert$	max|meas. - sim.|	length
(1)	-7.0 dB	-5.7 dB	0.7 dB	34.3 mm
(2)	-7.3 dB	-5.9 dB	0.7 dB	35.5 mm
(3)	-7.5 dB	-6.1 dB	0.3 dB	31.8 mm
(5)	-6.0 dB	-5.1 dB	0.8 dB	29.5 mm
(6)	-6.3 dB	-5.1 dB	0.8 dB	29.5 mm
(7)	-6.4 dB	-5.1 dB	0.5 dB	29.5 mm
(8)	-6.2 dB	-5.3 dB	0.8 dB	29.5 mm
(9)	-6.3 dB	-5.4 dB	0.9 dB	29.5 mm

A. *Feeding network sections*

All the measured feed network parts have similar performance. This is shown in Fig. 4 for the straight sections and missing vias, in Fig. 5 for the curved sections, and in Fig. 6 for the rat race balun. The measured transmission coefficients are listed in Table II. The table shows the highest and the lowest $|S_{21}|$ for each structure in the frequency band of 57 to 64 GHz. In addition, the table shows the maximum difference between the simulated and the measured $|S_{21}|$ and the length of the center conductor.

The structures show slight increase in losses as a function of frequency. Insertion loss of 0.14 to 0.17 dB/mm in the CBCPW and 0.5 dB for each connector based on -10 dB matching level are calculated from structure (5) measurements. The measured responses show small ripple caused by higher reflection coefficient when compared to the simulated parameters. Based on simulations, most of the losses are due to conductor surface roughness. Similar S_{21} in structures (5), (7), and (9) shows that the removal of one or two via pairs does not limit the usage of CBCPW lines. Thus a via removal can be used to cross CBCPW lines on different sides of the ground plane.

All prototype structures show the similar reflection coefficients (S_{11} and S_{22}) with periodic variations between -10 and -15 dB. These are caused by the previously mentioned gap on the conducting layers at the edge of the board. Based on the simulations, the proposed structures have low reflection coefficient, which is masked by the board edge issue. This is shown next in the antenna array time domain analysis.

Authorized licensed use limited to: Univ of Calif San Diego. Downloaded on January 03,2025 at 18:45:55 UTC from IEEE Xplore. Restrictions apply.

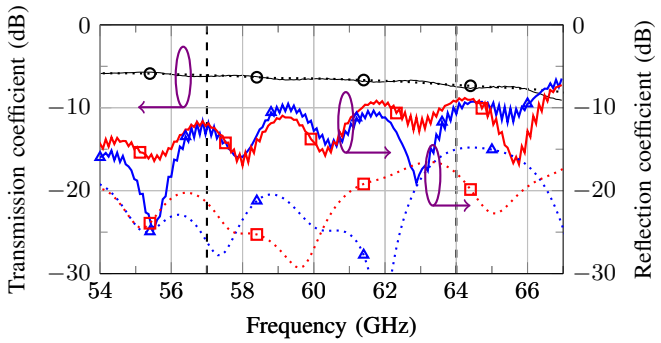

Fig. 6. Simulated (···) and measured (—) S-parameters for back-to-back rat-race balun (3). S_{21} ◯, S_{11} △, and S_{22} □ are shown.

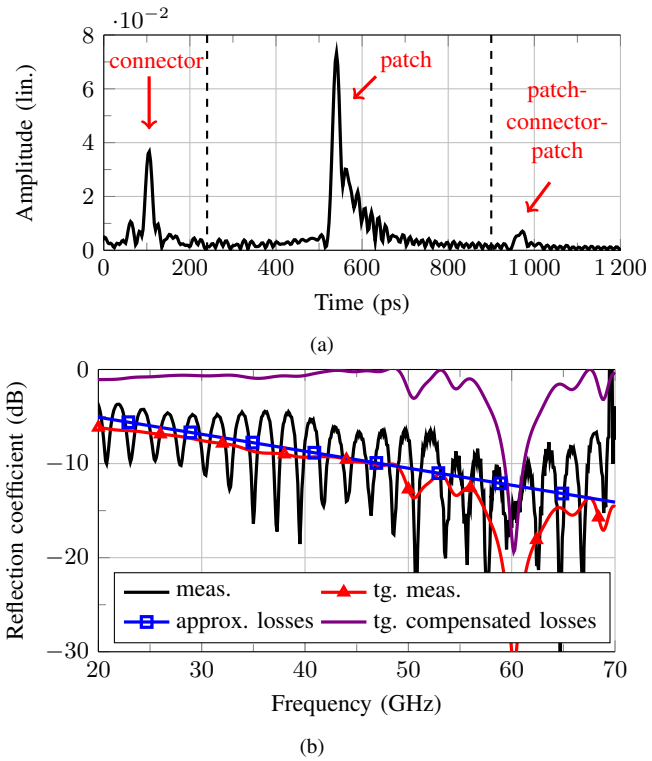

(a)

(b)

Fig. 7. (a) Time domain representation for S_{11} of antenna 1. The antenna response is shown between dashed lines representing the time gate. (b) Frequency domain presentation for measured S_{11}, time-gated S_{11}, time-gated and loss-compensated S_{11} , and the estimated loss.

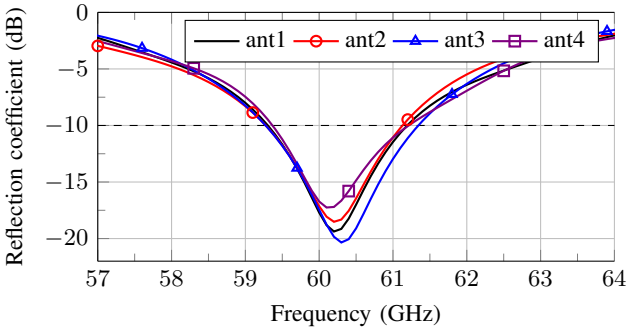

Fig. 8. Time-gated antenna S-parameters with de-embedded feed line losses.

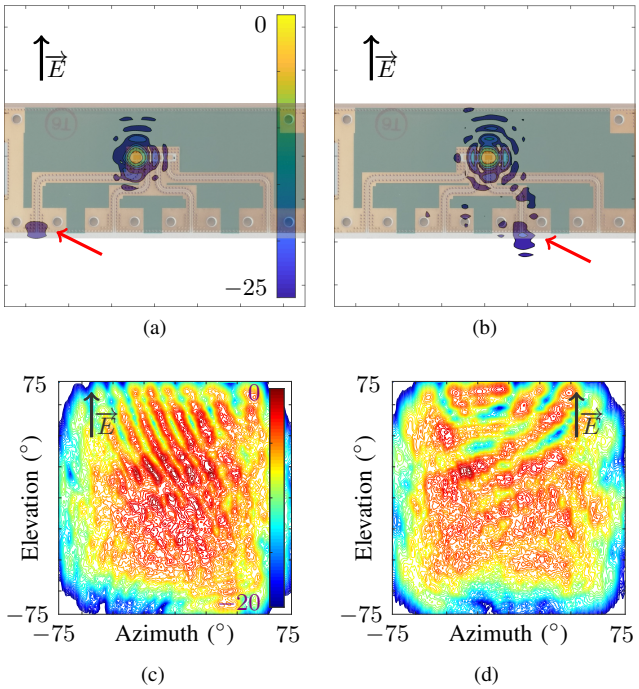

Fig. 9. Calculated hologram of (a) Antenna 1 and (b) Antenna 3 based on the near-field scanner data shows the unwanted radiation from the connectors (normalized field strength in dB). Normalized far-field pattern of (c) Antenna 1 and (d) Antenna 3 are obtained through near-field to far-field transformation. Scale in dB.

B. The antenna array

Antenna matching was determined by time-gating the measured reflection coefficient S_{11}. Fig. 7a shows the time domain information of the S_{11} of Antenna 1 measurement. Three reflections are visible. The first one is from the connector-PCB interface, the second one is from the patch itself, and the third one is the second reflection from the patch antenna. In the final SDR board the connectors are not present, therefore, only the first reflection from the patch is considered. The original and time-gated frequency responses can be seen in Fig. 7b. The patch antenna radiates only in a narrow band and, thus, the feed network losses can be extrapolated from the out-of-band area. The antenna matching is acquired by de-embedding these feed network losses. The same method is used for all four antennas. The results are shown in Fig. 8. The −10 dB bandwidth of the antenna elements is 1.76 GHz (from 59.4 to 61.1 GHz). Simulated feed line losses were 6.4 dB for Antenna 1 and 4, and 3.9 dB for Antenna 2 and 3. These were de-embedded when calculating the mutual coupling level of -14.7 dB and the realized gain for the antenna elements.

Far-field patterns were measured for each individual array element. During the far-field pattern measurements of elements 1 and 4, the connectors were attached only to ports 1 and 4 while ports 2 and 3 were open (and vice versa).

Two types of measurements were performed: far-field and near-field. The far-field measurements were done in an ane-

Authorized licensed use limited to: Univ of Calif San Diego. Downloaded on January 03,2025 at 18:45:55 UTC from IEEE Xplore. Restrictions apply.

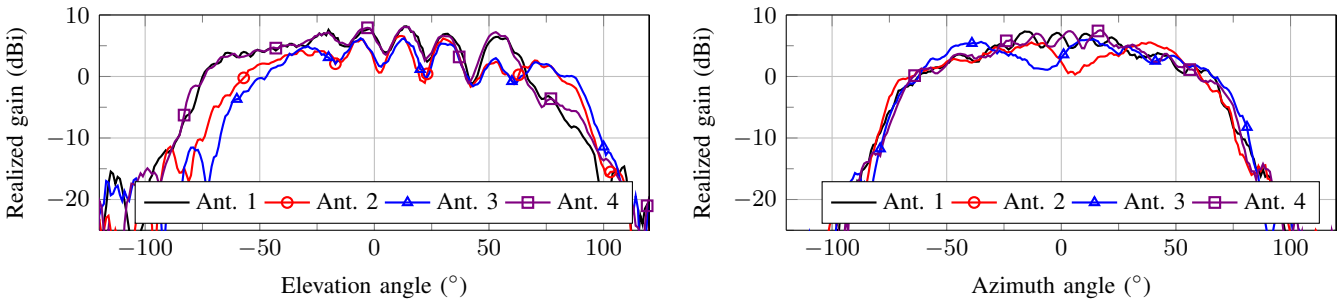

(a) (b)

Fig. 10. Measured far-field patterns with de-embedded feed line losses are shown at 60 GHz in (a) E-plane and in (b) H-plane.

choic chamber, whereas near-field measurements were done using planar scanner. The far-field pattern and the realized gain of the antenna elements are acquired through the far-field measurements, while a hologram image is obtained through the near-field measurements. The hologram image allows identifying unwanted radiation source in Fig. 9 from the connector located on the PCB.

Fig. 10a shows the far-field patterns in the E-plane and verifying the similar performance for all the elements. The middle elements have 1-2 dB higher realized gain than the edge elements. The beams of the middle elements are slightly tilted upwards in the elevation plane, whereas the edge elements radiate more towards the broadside. Differences are due to the middle elements being between two patches but edge elements are between patch and ground.

All these antennas share a similar ripple for elevation angle between $-20°$ and $75°$. Even low-level leakage from the connector can lead to high ripple as the antenna signal is attenuated by the feeding network before it radiates from the patch antenna, thus the relative difference is lower.

Far-field measurements in the H-plane are shown in Fig. 10b. Beam shape is similar for all the antenna elements. Edge elements have stronger ripple since there is a greater distance between the antenna element and the connector leakage. Magnitude of the ripple is approximately the same as in the E-plane for $0°$ elevation angle. For the center elements, the angular dependency of the ripple is lower, as the distance between the patch and connector in the azimuth plane is shorter. One can observe that the pairs of edge and center elements are approximately mirror images from each other.

IV. Conclusion

Patch antennas operating at 60 GHz and feeding network structures are studied. Measured S-parameters for every structure have similar transmission coefficient level and frequency dependency. Based on this, it can be verified that the limiting factor in the measurements is the transition from the connector to the PCB and not within the structure. In summary, these reflection coefficient levels will not affect the performance since the connectors would not be present in the SDR prototype.

Designed CBCPW feeding network parts and patch antenna elements can be used to construct an antenna array for fully digital SDR. Performance of the individual elements was verified by far-field and near-field measurements.

An additional resonance patch over current antenna design could be studied to provide wider frequency band while retaining simple design and low manufacturing cost. Future work also includes the system level measurements.

Acknowledgment

The authors are grateful to (Lic.Sc. (Tech.)) Mr. Matti Vaaja for assistance in the measurements. The work of V. Semkin was partly supported by a Jorma Ollila grant.

References

[1] M. Xiao *et al.*, "Millimeter wave communications for future mobile networks," *IEEE Journal on Selected Areas in Communications*, vol. 35, no. 9, pp. 1909–1935, Sep. 2017.

[2] T. S. Rappaport, Y. Xing, G. R. MacCartney, A. F. Molisch, E. Mellios, and J. Zhang, "Overview of millimeter wave communications for fifth-generation (5G) wireless networks—with a focus on propagation models," *IEEE Transactions on Antennas and Propagation*, vol. 65, no. 12, pp. 6213–6230, Dec 2017.

[3] Y. Ghasempour, C. R. C. M. da Silva, C. Cordeiro, and E. W. Knightly, "Ieee 802.11ay: Next-generation 60 GHz communication for 100 Gb/s wi-fi," *IEEE Communications Magazine*, vol. 55, no. 12, pp. 186–192, Dec 2017.

[4] I. Uchendu and J. Kelly, "Survey of beam steering techniques available for millimeter wave applications," *Progress In Electromagnetics Research B*, vol. 68, pp. 35–54, 2016.

[5] D. Raychaudhuri and N. B. Mandayam, "Frontiers of wireless and mobile communications," *Proceedings of the IEEE*, vol. 100, no. 4, pp. 824–840, April 2012.

[6] D. Kim, S. Park, T. Kim, L. Minz, and S. Park, "Fully Digital Beamforming Receiver With a Real-Time Calibration for 5G Mobile Communication," *IEEE Transactions on Antennas and Propagation*, vol. 67, no. 6, pp. 3809–3819, June 2019.

[7] K. Zheng *et al.*, "Software-defined radios to accelerate mmwave wireless innovation," in *2019 IEEE International Symposium on Dynamic Spectrum Access Networks (DySPAN)*, Nov 2019, pp. 1–4.

[8] R. Simons, *Coplanar Waveguide Circuits, Components, and Systems*, ser. Wiley Series in Microwave and Optical Engineering. Wiley, 2004.

[9] C. Eu Guan, K. Yoshitomi, and H. Kanaya, "Derivation of the optimum distance between periodically spaced vias for leakage suppression at s-band," *Microwave and Optical Technology Letters*, vol. 58, no. 5, pp. 1257–1260, 2016.

[10] D. Pozar, *Microwave Engineering*. Wiley, 2011.

[11] W. L. Stutzman and G. Thiele, *Antenna theory and design*. J. Wiley, 1998.

[12] Advanced Connectivity Solutions, "Copper foils for high frequency materials," Rogers Corporation, Tech. Rep., 2019.

Authorized licensed use limited to: Univ of Calif San Diego. Downloaded on January 03,2025 at 18:45:55 UTC from IEEE Xplore. Restrictions apply.